2001

Deactivation of Thermally Formed Ru/Ti Oxide Electrodes. An AC Impedance Characterization Study

Birss, Viola I.; Tilak, B. V.; Wang, J.; Chen, C.-P.; Rangarajan, S. K.

The Electrochemical Society

Tilak, B. V., Birss, V. I., Wang, J., Chen, C.-P. and Rangarajan, S. K. (2001). "Deactivation of Thermally Formed Ru/Ti Oxide Electrodes. An AC Impedance Characterization Study". Journal of the Electrochemical Society, Vol. 148(9): D112-D120.

http://hdl.handle.net/1880/44731

journal article

Journal of The Electrochemical Society, **148** (9) D112-D120 (2001)
0013-4651/2001/148(9)/D112/9/$7.00 © The Electrochemical Society, Inc.

Deactivation of Thermally Formed Ru/Ti Oxide Electrodes

An AC Impedance Characterization Study

B. V. Tilak,[a,*] V. I. Birss,[b,*,z] J. Wang,[b] C.-P. Chen,[c] and S. K. Rangarajan[d]

[a]*Grand Island, New York 14072, USA*
[b]*Department of Chemistry, University of Calgary, Calgary T2N 1N4, Canada*
[c]*Occidental Chemical Corporation, Grand Island, New York 14072, USA*
[d]*Raman Research Institute, Bangalore 560080, India*

Freshly formed Ru/Ti oxide anodes, containing between 5 and 40 atom % Ru, have been examined for their Tafel behavior during chlorine evolution, as well as their cyclic voltammetric (CV) and ac impedance response at the open-circuit potential, in chlorine-free NaCl solutions. Also, 30 atom % Ru electrodes have been electrochemically deactivated, as seen by an increase in the anode potential and the Tafel slope for the chlorine evolution reaction during long-term electrolysis. A comparison of the data for the fresh and the deactivated anodes suggests that the deactivated anodes have similar electrochemical characteristics as freshly formed, low-Ru-content (*ca.* 5 atom %) oxide films. To understand this better, the experimentally obtained ac impedance data were compared to the calculated impedance, based on a porous film model in which a one-electron surface redox reaction occurs. While the fit is good at medium-to-high frequencies, the inclusion of a diffusion-controlled process for the low atom percent Ru films is required to achieve a good fit also at low frequencies. Taken together, these results support the hypothesis that the deactivation of originally high atom percent Ru anodes is due to the depletion of Ru from the oxide film, causing its electrochemical behavior to become more similar to that of freshly formed low atom percent Ru oxide films.
 [DOI: 10.1149/1.1388630]

Manuscript submitted January 4, 2001; revised manuscript received April 20, 2001. Available electronically August 10, 2001.

Ru/Ti oxide anodes, formed by thermal decomposition techniques on titanium substrates and used in the chlor-alkali industry, typically contain >30 atom % RuO_2, the remaining being TiO_2.[1,2] The Ru metal loading in these oxide mixtures is generally in the range of 4-10 g/m^2, depending on whether their use is in diaphragm or in membrane (or chlorate) cells. Ru/Ti oxides of this composition typically exhibit chlorine evolution overpotentials of 40-60 mV at 200-250 mA/cm^2 in 5 M NaCl solutions at 80-90°C. However, with extended usage in cells in practice, the chlorine overpotential sometimes increases to 300-400 mV, and the anode is considered to have become ''deactivated.'' This is clearly an undesirable situation, and hence, the focus in this paper is to understand the origin of anode deactivation more clearly.

The possible mechanisms relevant to the deactivation of RuO_2/TiO_2-based anodes during the course of the chlorine (and oxygen) evolution reactions have been the subject of several recent reviews[1-3] and various publications.[4-24] One possible cause of anode deactivation is a loss of active sites for chlorine evolution by blockage of insoluble surface layers (*e.g.*, MnO_2, $BaSO_4$, Fe oxides, etc.) or impurities (*e.g.*, organics) which arise from impurities in the feed brine to the cells.

Another possibility is the formation of an insulating TiO_2 layer at the Ti/coating interface with time of anodic polarization,[8-10,24] although there is no direct supporting evidence for this hypothesis. A further option is that a loss of Ru occurs from the coating, either throughout the film or only at its outer surface.[9,12,20,23,25] This may take place by erosion and/or dissolution, or via the loss of Ru-based adsorbed intermediates participating in the chlorine and oxygen evolution reactions. In support of the suggested loss of Ru, it is known that a notable increase in the resistivity of mixed Ru/Ti oxides occurs[26-30] when the RuO_2 content is <20 atom %.

Focusing on the latter explanation, it is unequivocally agreed that during electrolysis some RuO_2 does dissolve electrochemically (although the magnitude of the rate of dissolution is not known with certainty) and that some of it is also lost by erosion.[4,6] The corrosion rate of RuO_2 is minimal at pH 1-2[12,16] and increases below a pH of *ca.* 0.2 (forming $RuOHCL_5^{2-}$)[12] and above a pH of *ca.* 4 (forming RuO_4^{2-} and gaseous RuO_4.[7,8,19,31] The RuO_2 dissolution rate increases with increasing current density,[7,9] increasing the percentage of O_2 generation,[5,18,19] decreasing NaCl concentration,[11,21] and an increasing number of shutdowns of operating cells.[7,17] TiO_2 dissolution is believed to be chemical,[15] resulting in the formation of TiO^{2+}.

The purpose of the present communication is to provide a better understanding of the causal factors leading to the large chlorine evolution overpotentials seen at deactivated anodes, with the ultimate hope of developing preventive measures which would extend their operating life in practice. Another objective of this work is to demonstrate that the impedance response of a Ru/Ti oxide film over a wide range of frequencies may serve as an excellent indication of the extent of its deactivation. In this paper, the electrochemical behavior of freshly formed Ru/Ti oxides containing varying amounts of Ru was established. This was achieved by collecting the chlorine evolution Tafel data and comparing this to the cyclic voltammetric and ac impedance response in chlorine-free NaCl solutions. Anodes which were 30-40% in their original Ru content were then deactivated using a range of aggressive current/potential/time regimes in various solutions. It is shown by modeling of the ac impedance data for both fresh and deactivated oxide electrodes, and assuming a porous film structure, that the deactivated 40 atom % Ru electrodes behave very similarly to freshly formed Ru/Ti oxide electrodes containing small amounts of Ru (<5%). This suggests that the depletion of Ru from the mixed oxide is indeed responsible for the high anode potentials following the deactivation of the electrodes. Complementary data presented elsewhere,[32] based on the use of nonelectrochemical techniques such as secondary-ion mass spectrometry (SIMS) and scanning tunneling microscopy (STM),[33] have also supported the dissolution of Ru[32] as the explanation for anode deactivation.

Experimental

Electrodes for cyclic voltammetry and ac impedance experiments.—The working electrodes (WEs) consisted of Ti wire substrates (99.99%, Johnson-Matthey, Inc., 2 mm diam), upon which the Ru/Ti oxide films were deposited. The cross-sectional end of each bare Ti wire (0.0314 cm^2) was polished with 600 grit paper, rinsed with acetone, dried, rinsed with methylene chloride, dried again, and then rinsed with triply distilled water before coating with oxide. Ru(III) chloride (18.2 g, Johnson Matthey, Mallory, Ltd.) Ti(IV) butoxide (45 mL, Aldrich), and 37% HCl (6 mL) were mixed together to make the stock coating solution. Solutions of different

* Electrochemical Society Active Member.
z E-mail: birss@ucalgary.ca

Ru and Ti content were made by adding the appropriate amount of Ti butoxide to the stock solution. The Ti electrodes were dipped into this solution and allowed to air-dry to form a single layer of oxide film. The electrodes were then heated at *ca.* 5°C per min to 100°C, remaining there for *ca.* 15 min to remove the solvent. The temperature was then increased at 10°C/min to 440°C in air and maintained at 440°C for 30 min to decompose the Ru/Ti compounds, thus forming the mixed Ru/Ti oxide, *ca.* 2 μm thick. Afterward, the length of the oxide-coated Ti wire was wrapped in Teflon tape, leaving only the cross-sectional end as the WE for immersion in solution.

The counter electrode (CE) was a 40 atom % Ru (the remainder being Ti oxide) oxide electrode, having more than 100 times the apparent surface area of the WE. It was positioned inside a Teflon tube to promote the release of hydrogen gas from the cell. An Ag/AgCl electrode was employed as the reference electrode (RE) at high temperatures, while a standard calomel electrode (SCE) generally served as the RE at room temperature.

Equipment.—An EG&G PARC 273 potentiostat/galvanostat was used in both the electrolysis and the CV experiments, coupled with an HP 7044 B X-Y recorder. A Solartron 1255 HF frequency response analyzer and a Solartron 1286 electrochemical interface were employed for the ac impedance measurements, using frequencies from 0.1 to 65 kHz and a 10 mV ac amplitude (effective) at either the open circuit potential (OCP) or at various applied potentials. As the RE can introduce a time delay at high frequencies, observed as a phase shift due to its resistance and capacitance characteristics, an additional Pt wire electrode was placed in the cell and was connected via a 6.8 μF capacitor to the RE lead.[34-36]

Solutions and general experimental conditions.—The solution used for all experimentation was 5 M NaCl, made up using triply distilled water. Electrolysis experiments were carried out in a one-compartment cell at either room temperature or at 90°C. All CV and impedance experiments were carried out using a two-compartment cell, with the RE compartment connected to the WE and CE compartments via a Luggin capillary.

Ru/Ti oxide deactivation procedures.—It was found that anode deactivation by the application of a constant anodic current density of between 200 and 250 mA/cm^2 in 5 M NaCl (pH maintained at 3-5) required many days. Therefore, it was found to be more effective to deactivate the anodes in an acidified salt solution (5 M NaCl + 0.1 M HCl). This was done either by applying a constant anodic current density, by square wave current cycling (+320 to −130 mA/cm^2, 30 s for each pulse), by cycling (100 mV/s) the overpotential between *ca.* +1 and *ca.* −0.5 *vs.* the OCP, or by the application of square wave (30 s) potential cycles (1.35 to −0.3 V *vs.* SCE).

Results

Tafel data for fresh and deactivated Ru/Ti oxide electrodes during chlorine evolution.—Figure 1 depicts the time dependence of the chlorine overpotential (measured intermittently at 230 mA/cm^2), observed when a 40 atom % Ru electrode was subjected to overpotential cycling in the range 900 to −600 mV in 5 M NaCl at 90°C. The overpotential was found to increase from an initial value of *ca.* 70 mV (often lower values close to 40 mV are seen) to more than 400 mV. Similar phenomena were also observed by using square-wave current cycling from 320 mA/cm^2 to −130 mA/cm^2 (30 s pulse duration) in 5 M NaCl + 0.1 M HCl solutions at 90°C.

To better understand Fig. 1, the chlorine evolution Tafel plots at freshly 5-40 atom % Ru/Ti oxide electrodes, prior to deactivation, are shown in Fig. 2a at room temperature. These plots show, as observed previously,[13,37] increasing Tafel slopes and a decrease in the i_o values for the chlorine evolution reaction as the Ru content of the oxide coating is lowered. The Tafel slope is *ca.* 30-40 mV for the 30-40 atom % Ru electrodes, while for the 5 atom % Ru oxide, it has increased to *ca.* 130 mV. The reasons for this behavior are discussed in detail in Ref. 37, in terms of a decreasing number of active

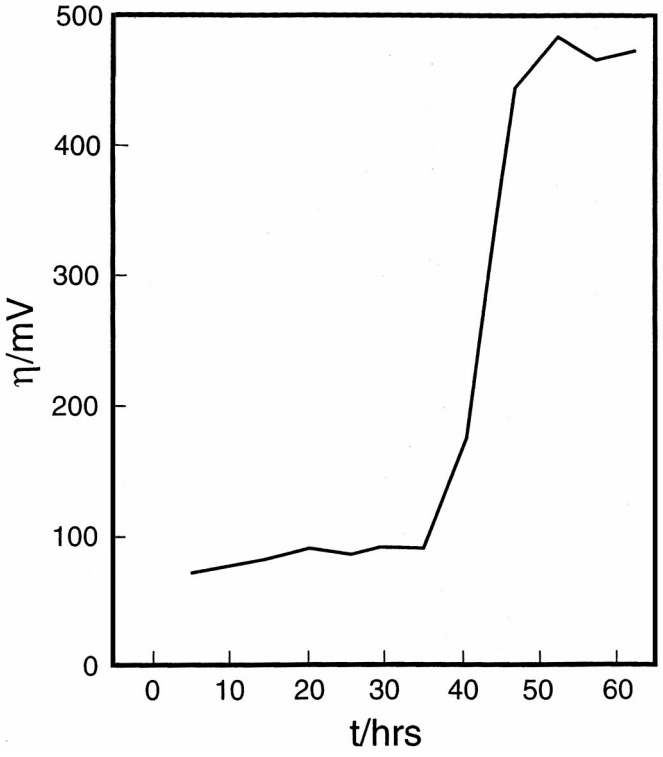

Figure 1. Time dependence of overpotential of 40 atom % Ru electrode (*ca.* 2 μm in thickness) at 230 mA/cm^2 in 5 M NaCl at 90°C. Electrode subjected to overpotential cycling from 900 to −600 mV at 10 mV/s.

Ru sites with decreasing atom percent Ru, resulting in a decrease in i_o values for the chlorine evolution reaction. The increasing Tafel slope may be due to an increasing surface coverage of the adsorbed intermediate, varying from close to zero on a 40 atom % Ru electrode to unity on a 5 or 10 atom % Ru oxide electrode. Alternatively, this change in slope may arise from an increase in the film resistance of the Ru/Ti electrodes with time of chlorine evolution.

The Tafel plots for the chlorine evolution reaction, collected at various times between deactivation by periods of square-wave potential cycling (1.35 to −0.32 V *vs.* SCE, 60 s/cycle) are shown in Fig. 2b. Overall, it can be seen that the activity of these electrodes decreases with time of deactivation. At early times, some increase in activity is sometimes seen, arising, at least in part, from an increased electrode surface area as loosely attached oxide particles are lost from the surface. Subsequent profiles show a slowly increasing Tafel slope and a decreasing i_o value with increasing time of electrolysis. At between 33 and 37 h of electrolysis, a sharp increase in the *b* value is seen, reaching *ca.* 150 mV.

A comparison of the data in Fig. 2a and b, summed up in Fig. 3a and b, shows that after the anode is subjected to long times of potential or current cycling, a 40 atom % Ru electrode behaves similarly to a <5 atom % Ru electrode. This already strongly suggests that Ru dissolution is occurring from the coating in these experiments.

CV response of fresh and deactivated electrodes.—The CV features (Fig. 4a) of the 40 atom % Ru/Ti oxide electrodes before, during, and after deactivation (achieved by current pulsing between 0 and 0.955 A/cm^2) were monitored from 0.5 to 1.0 V *vs.* Ag/AgCl at 100 mV/s in fresh 5 M NaCl solution (pH 3-5) at 90°C. These potential limits were chosen to avoid any faradaic interference due to the occurrence of the chlorine, oxygen, and hydrogen evolution/reduction reactions.

It can be seen that the fresh electrode (——) gives the typical pseudocapacitive response of Ru oxide,[38,39] changing reversibly

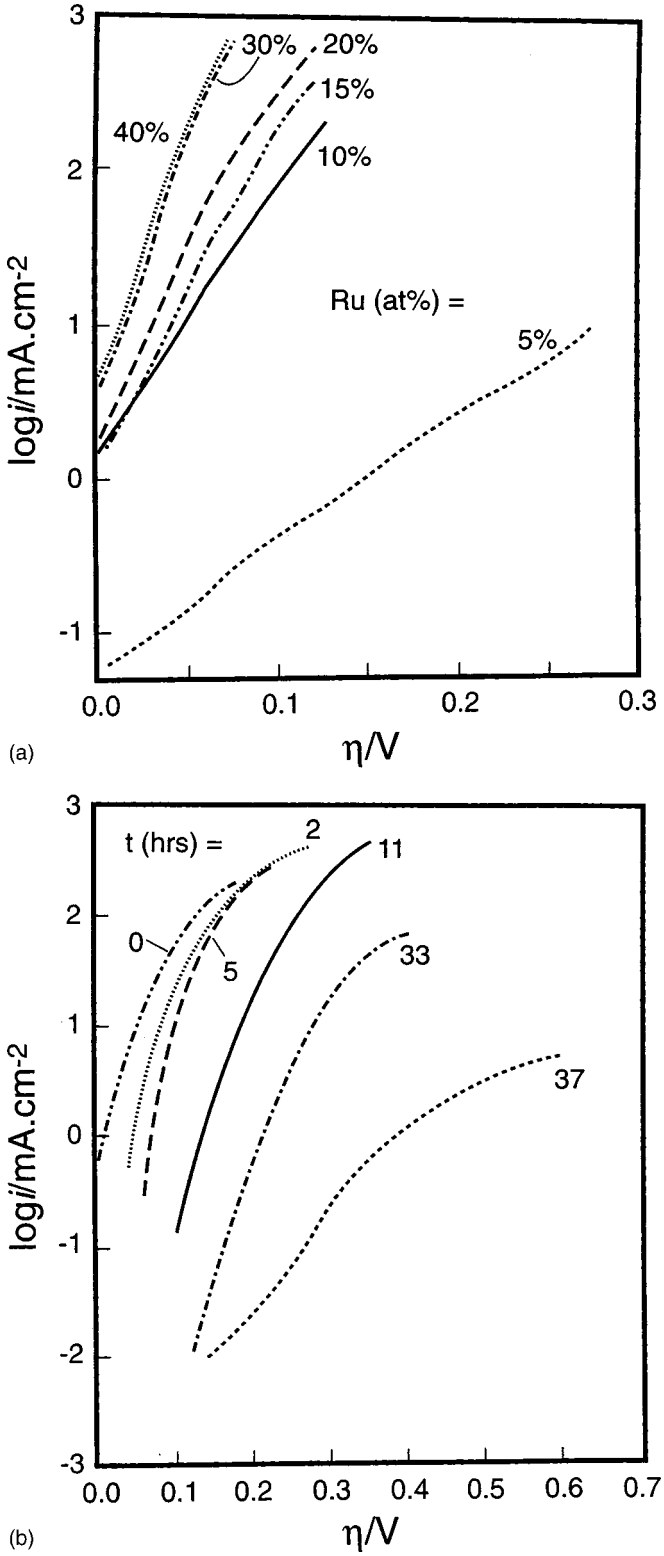

Figure 2. (a, top) Effect of Ru content on Tafel plot of fresh Ru/Ti electrodes in 5 M NaCl (pH~3.5) at room temperature (with IR compensation). (b, bottom) Time dependence of chlorine evolution Tafel data at 40 atom % Ru electrode at room temperature (without IR compensation), subjected to deactivation by square-wave potential cycling (1.35 to −0.32 V *vs.* SCE at 60 s/cycle) in 5 M NaCl+0.1 M HCl. The numbers in the figure refer to the time of deactivation in hours. Each Tafel plot is shifted to the right by 20 mV to avoid overlap.

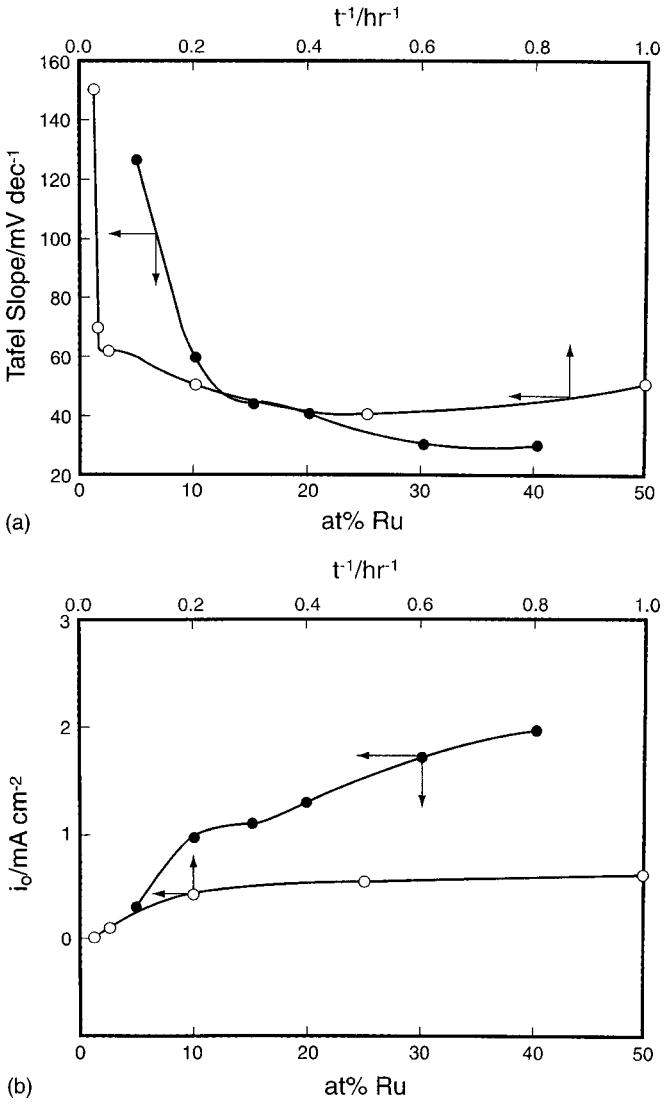

Figure 3. (a, top) (●) Tafel slope variation with atom % Ru on fresh electrodes and (○) of a 40 atom % Ru electrode subjected to deactivation. (b, bottom) (●) Exchange current density with atom % Ru on fresh electrodes and (○) of a 40 atom % Ru electrode subjected to deactivation.

when the direction of potential cycling is changed. A decrease of up to a factor of 5 is observed in the response after *ca.* 70 h of deactivation. The CV response of fresh electrodes of various Ru contents at 90°C is shown in Fig. 4b for comparison. Consistent with the literature,[13] the pseudocapacitive response decreases sharply when the Ru content of the oxide is below *ca.* 10 atom %, while there are no significant differences in the response of electrodes containing 20-40 atom % Ru, other than a loss of capacity. By comparing the CV response of fresh electrodes of relatively low Ru content (Fig. 4b) with the response of the 40 atom % Ru electrode after long times of electrolysis (Fig. 4a), there is again strong evidence that the Ru concentration decreases substantially with time of electrolysis. This may occur either only at the oxide surface or throughout its bulk.

AC impedance behavior of fresh and deactivated Ru/Ti oxides.—To further understand and characterize the oxide deactivation process, ac impedance studies were carried out, focusing primarily on a 30 atom % Ru/Ti electrode at various stages of deactivation. These data were compared to those obtained for freshly formed Ru/Ti oxide films, ranging in Ru content from 5 to 40 atom %. Impedance data were collected at the oxide OCP (*ca.* 0.9 V *vs.* SCE)

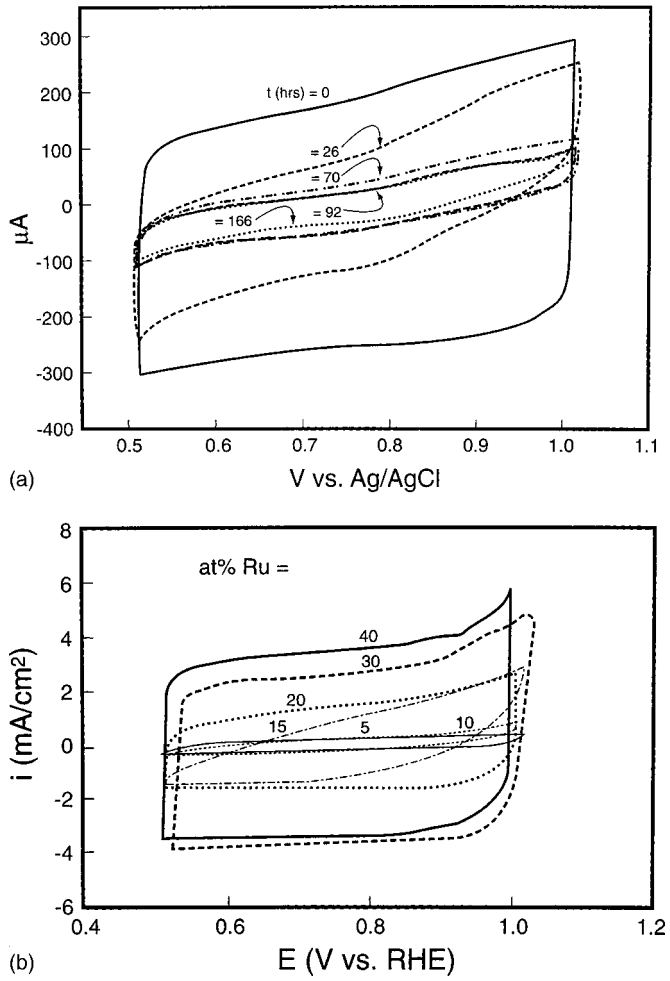

Figure 4. (a, top) Cyclic voltammograms (CVs, at 100 mV/S, 0.1 cm^2 electrode area) of a 40 atom % Ru-Ti electrode in 5 M NaCl (pH ~ 3.50) after various times of deactivation at 90°C. (b, bottom) CVs of fresh Ru-Ti electrodes with different Ru content (*ca.* 2 μm thick) in 5 M NaCl (pH ~ 3.5) at 100 mV/s at 90°C.

in chlorine-free NaCl solutions. Under these conditions, no chlorine reactions can occur and the OCP is defined by the Ru/Ti oxide surface electrochemistry. In these experiments, deactivation was generally accomplished by square-wave potential cycling, using overpotentials *vs.* the chlorine/chloride potential of *ca.* 1.6 to −0.1 V (60 s/cycle) in 5 M NaCl + 0.1 M HCl solutions at room temperature.

The impedance and phase angle Bode plots, obtained during the course of deactivation of a 30 atom % Ru electrode, are presented in Fig. 5. For comparison, the impedance response[37] for freshly formed Ru/Ti oxide electrodes containing varying amounts of Ru is shown in Fig. 6. It is seen that the phase angle plots are the most sensitive to the Ru content of the films, as compared to the impedance Bode plots or to Nyquist plots. During the initial stages of deactivation, the phase angle plot of the 30 atom % Ru electrode (Fig. 5) shows the close-to-ideal capacitive behavior seen for freshly formed 30 or 40 atom % Ru electrodes (Fig. 6), as expected. However, after over 1 h of deactivation, the phase angle plots (Fig. 5) begin to reveal a peak in the high-frequency range, and a phase angle of 50-70° develops at lower frequencies. The impedance increases significantly, as seen at low frequencies, from *ca.* 10 Ω to more than 500 Ω after *ca.* 2 h of deactivation by potential cycling. A comparison of the results of Fig. 5 (after more than 1 h of deactivation) with those of Fig. 6 indicates clearly that the impedance response of the fresh 30

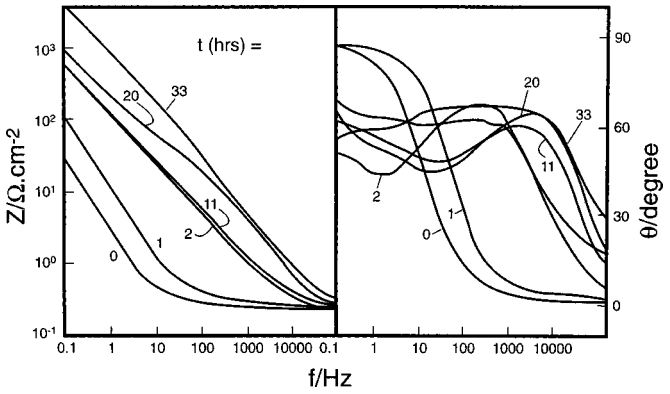

Figure 5. Impedance response of 30% Ru electrodes after various times of deactivation in 5 M NaCl + 0.1 M HCl at room temperature. Electrode subjected to square potential cycling from 1.35 to −0.32 V *vs.* SCE at 60 cycles/s. Impedance measured in 5 M NaCl at room temperature at OCP.

atom % Ru electrode becomes more similar to that of freshly prepared 5-10 atom % Ru oxide coatings with time of deactivation.

The most important aspect of Fig. 6 is that the impedance plots for freshly formed Ru/Ti oxide films reveal "the signature" of the Ru content of the electrodes, indicating their possible use as a "diagnostic" tool for partially or fully deactivated electrodes. The diagnostics include

1. The monotonic decrease of the impedance amplitude $|Z|$ as a function of frequency, ω.
2. The transition from convexity to concavity in the $|Z|$ *vs.* ω plots as a function of increasing Ru content.
3. The appearance of a pronounced maximum at low Ru contents in the phase angle *vs.* ω plots.
4. The tendency for capacitive behavior at low ω for higher Ru content.
5. The tendency for Warburg-like behavior at low ω for low-Ru-content electrodes.
6. Asymptotically, for ω→0 and low Ru content, $|Z| \sim 1/\sqrt{\omega}$.
7. Asymptotically, for high Ru content, $|Z| \sim 1/\omega$ as $\omega \rightarrow 0$.

It is clear that the impedance response arises from several different processes, which are dominant in different frequency or time domains. Separation of these processes is difficult, and hence the treatment described is intended to analyze the data in approximate ranges of frequency/parameter space.

Theory

In order to model the impedance data shown in Fig. 5 and 6, three important aspects of the Ru/Ti oxide film must be kept in

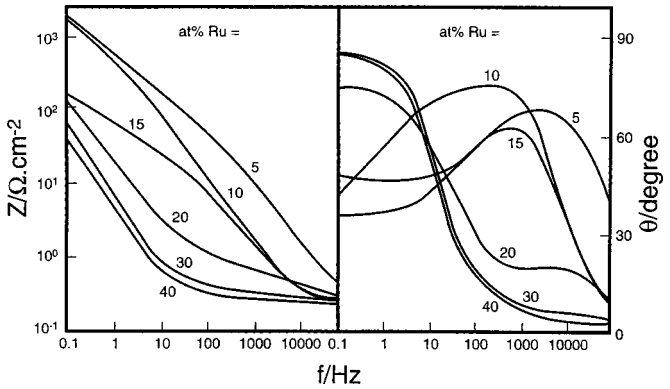

Figure 6. Impedance response of fresh electrodes of different Ru contents in 5 M NaCl at room temperature at OCP.

mind: (*i*) the pseudocapacitive nature of the electrode process occurring at the surface of the Ru oxide under the conditions of our experiment, as described by

$$2RuO_2 + 2H^+ + 2e^- \leftrightarrow Ru_2O_3 + H_2O \qquad [1]$$

(*ii*) the spatial distribution of the potential with depth into the film (moreso once the Ru content drops below *ca.* 20%, when its conductivity decreases rapidly); and (*iii*) the heterogeneous nature of the active sites in the film (describing the compositional and porosity variations across the thickness of the film). The important phenomenological components of the system under study are the double layer at the oxide/solution interface, the electrochemical activity of the Ru sites (in the absence of other reactions such as chlorine evolution), and the distribution of potential in the film. The primary variables are, then, the specific double-layer capacitance, C_d; the exchange current density associated with Reaction 1 and the concentration of the Ru(IV)/Ru(III) species in the film (cf. Eq. 1); and the specific conductivity of the film (ρ_f) and of the solution (ρ_e).

We assume that during the impedance experiments at the OCP in chlorine-free chloride solutions, there is no pH variation in or near the oxide film, and that the diffusion of Ru(IV)/Ru(III) sites in the film via exchange mechanisms is extremely slow at the frequencies studied. However, the Ru(IV)/Ru(II) ratio in the film is influenced by the potential change during impedance measurements, as seen from Reaction 1. We term the Ru(IV) and Ru(III) surface activities as Γ_O and Γ_R, respectively, and the overpotential of the electrode, η, is defined *vs.* the OCP during impedance measurements. The faradaic current, i_Γ, associated with Reaction 1, may be written as

$$i_\Gamma = i_o\left(\frac{\Gamma_O}{\Gamma_O^o}e^{\alpha nf\eta} - \frac{\Gamma_R}{\Gamma_R^o}e^{-(1-\alpha)nf\eta}\right) \qquad [2]$$

where i_o, the exchange current density, is pH-dependent, $f = F/RT$, and α is the familiar transfer coefficient. With alternating signal perturbation, we may write Eq. 2 in a linearized form, as shown in

$$\delta i_\Gamma = i_o\left(\frac{\delta\Gamma_O}{\Gamma_O^o} - \frac{\delta\Gamma_R}{\Gamma_R^o} + nf\delta\eta\right) \qquad [3]$$

Because

$$\delta i_\Gamma = -nF\frac{d\delta\Gamma_O}{dt} = nF\frac{d\delta\Gamma_R}{dt} \quad (i.e., \delta\Gamma = -\delta\Gamma_R) \qquad [4]$$

Eq. 3 can be recast as

$$\delta i_\Gamma = i_o\left[\left(\frac{1}{\Gamma_O^o} + \frac{1}{\Gamma_R^o}\right)\delta\Gamma_O + nf\delta\eta\right] \qquad [5]$$

The frequency dependence of $\delta\Gamma_O$ is given through Eq. 4 and 5, after Laplace transformation, as

$$\delta\Gamma_O = -i_o nf\delta\eta\left[\left(\frac{1}{\Gamma_O^o} + \frac{1}{\Gamma_R^o}\right)i_o + nFP\right]^{-1} \qquad [6]$$

where $p = j\omega$, $j = \sqrt{-1}$, and ω is the angular frequency. Equation 6 implies that the dominant spatial variation of $\delta\Gamma_O$ is via its dependence on $\delta\eta(x)$ and not via a "diffusion" path. It follows from Eq. 6, using the proper sign convention, that

$$C_\phi = nF\left(\frac{\delta\Gamma_O}{\delta\eta}\right)_{p\to 0} = \frac{n^2F^2}{RT}\left[\left(\frac{1}{\Gamma_O^o} + \frac{1}{\Gamma_R^o}\right)i_o\right]^{-1} \qquad [7]$$

where C_ϕ is the pseudocapacitance associated with Reaction 1.

Equation 6, when substituted into Eq. 5, gives the linear response valid for a planar electrode for Reaction 1. Figure 7 (circuit A) shows the appropriate equivalent circuit (also see Ref. 40) for this case; however, since Ru/Ti oxide films are three dimensional and porous, our analysis must reflect this feature. Therefore, the flooded porous model (see Ref. 40-44 for details), which includes the potential distribution across the film, is employed here. The equation giving the potential distribution across the film, $\delta\eta(x)$, for a porous electrode for the sinusoidal case is now given, where x is the distance into the film from the film/solution interface

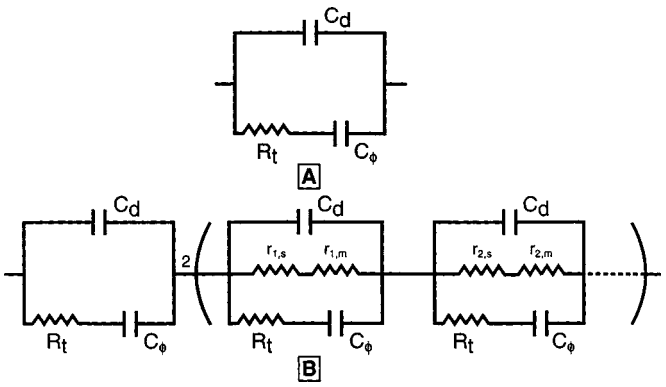

Figure 7. Theoretical equivalent circuits for Reaction 1 at a planar electrode [A] and a porous electrode [B].

$$p\delta\eta = \frac{\sigma'}{C_d}\frac{\partial^2\delta\eta}{\partial x^2} - \frac{\delta i_\Gamma}{C_d} \qquad [8]$$

In this equation, C_d and σ' denote the specific capacity of the double layer and the total conductivity of the medium (sum of electrode matrix and electrolyte), respectively. The local current, δi_Γ, at depth x into the film, due to Eq. 1, is therefore

$$\delta i_\Gamma(x) = \frac{pnF}{R_t}\left[pnF + i_o\left(\frac{1}{\Gamma_O^o} + \frac{1}{\Gamma_R^o}\right)\right]^{-1}\delta\eta(x) \qquad [9]$$

where $R_t = RT/nFi_O$. Equation 9 is then substituted into Eq. 8 and the differential equation for $\delta\eta(x)$ is solved, using the following boundary conditions at $x = 0$ (at the outer film/solution interface) and 1 (at the film/underlying metal interface)

$$\frac{\partial\delta\eta}{\partial x} = 0 \quad \text{at } x = 0 \qquad [10]$$

$$\frac{\partial\delta\eta}{\partial x} = \frac{1}{\sigma' S}\delta I \quad \text{at } x = l \qquad [11]$$

where δI is the sinusoidal current amplitude and S is the specific surface area of the oxide film. The overall impedance for the porous Ru/Ti oxide electrode is therefore obtained, following the procedures in Ref. 40, as

$$Z_p(p) = R_e\frac{\coth U(p)}{U(p)} \qquad [12]$$

where $R_e = l/\sigma' S$. In Eq. 12, $U(p)$ is given by

$$U(p) = \sqrt{\frac{1}{\sigma''}\left(p\tau_1 + \frac{p\tau_2}{p\tau_3 + 1}\right)} \qquad [13]$$

where $\sigma'' = l/S$. The time constants, τ_1, τ_2, and τ_3, are defined as

$$\tau_1 = R_eC_d \quad \tau_2 = R_eC_\phi \quad \tau_3 = R_tC_\phi \qquad [14]$$

where R_e, R_t, C_ϕ, and C_d have their previous definitions. The equivalent circuit corresponding to the impedance function in Eq. 12 for a porous electrode is shown in Fig. 7 (circuit B).[40]

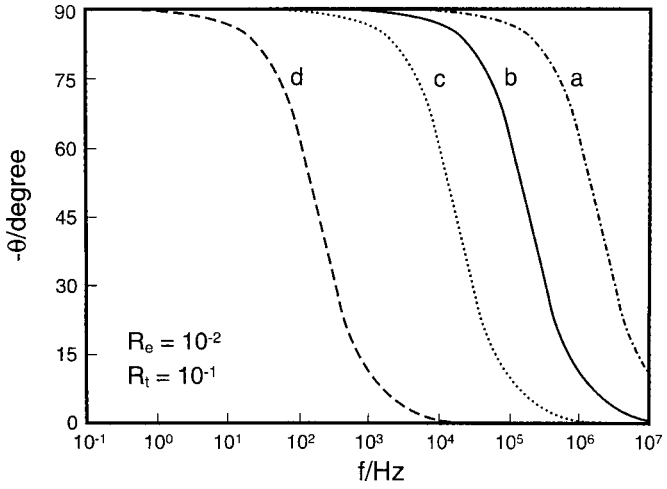

Figure 8. Calculated phase angle impedance data using Eq. 12 and 13 for $R_e = 10^{-2}$.

	C_d	C_φ	R_t
(a)	10^{-7}	10^{-8}	10^{-1}
(b)	10^{-6}	10^{-8}	10^{-1}
(c)	10^{-6}	10^{-5}	10^{-1}
(d)	10^{-6}	10^{-3}	10^{-1}

The experimentally measured impedance, Z_T, includes an additional series resistance component, R_x (the resistance between the WE and the RE, which is external to the porous electrode), and thus

$$Z_T = R_x + Z_p \qquad [15]$$

Discussion

The rich features which are observed in the impedance data, especially in the phase angle plots (Fig. 5 and 6), are a reflection of the interplay of processes which are occurring in different time (or frequency) domains. Unfortunately, there is no simple equation which arises from the impedance function (Eq. 12), which yields the maxima and minima in the phase angle plots. Therefore, we illustrate how the presence of the three time constants described can lead to the distinct features in the phase angle plots. This is done by examining the effect of two limiting cases on Eq. 12 in the following treatment.

Dependence of impedance response on frequency.—Case 1 ($\tau_3 = R_t C_\phi \ll 1$).—When τ_3 is small, i.e., when $C_\varphi \ll 1$ or when the charge-transfer resistance for Reaction 1 is small (these conditions could be met for thin, conducting Ru-rich oxide films), Eq. 15 becomes

$$Z_T = R_x \text{ when the impedance is resistive as } \omega \to \infty \qquad [16]$$

and

$$Z_T = R_x + \frac{R_e}{p(C_d + C_\phi)}$$

$$\text{when the impedance is capacitive as } \omega \to 0 \qquad [17]$$

This behavior is illustrated in Fig. 8, for various values of C_d and C_ϕ, while maintaining $R_t C_\phi \ll 1$. It can be seen that as the magnitude of $(C_d + C_\phi)$ increases, the time constant increases, and as a result, the phase angle reaches 90° at longer times or at lower frequencies, as is observed for 30 and 40 atom % Ru electrodes in Fig. 6.

Case 2.—Here the limiting results are presented when the relative magnitudes of the time constants are such that the following inequalities apply, $\omega_a \gg \omega_c \gg \omega_b$, *i.e.*, when $[R_e(C_d + C_\phi)]^{-1} \gg (R_t C_d)^{-1} \gg (R_t C_\phi)^{-1}$, where

$$\omega_a = (\tau_1 + \tau_2)^{-1}, \quad \omega_b = \tau_3^{-1}, \quad \omega_c = (\tau_1 \tau_3 / \tau_2)^{-1} \qquad [18]$$

This situation is possible when the charge-transfer resistance is large, as would be the case for lower (<20) atom % Ru electrodes.

1. At very low frequencies, *i.e.*, for $\omega \ll \omega_b$

$$Z_T \sim R_x + \frac{R_e}{p(\tau_1 + \tau_2)} \sim R_x + \frac{1}{p(C_d + C_\phi)} \qquad [19]$$

and the impedance is capacitive.

2. For the same sequence of time constant magnitudes but at intermediate frequencies, *i.e.*, when $\omega_b < \omega \ll \omega_c \ll \omega_a$, then

$$Z_T \sim R_x + R_e / \sqrt{p\tau_1 + \tau_2/\tau_3}$$
$$= R_x + R_t / \sqrt{p/\omega_c + 1} \quad (\text{when } \tau_2/\tau_3 < 1)$$
$$\sim R_x + R_t \qquad [20]$$

As ω increases to satisfy the inequality, $\omega_b \ll \omega_c \ll \omega \ll \omega_a' = \tau_1^{-1}$

$$Z_T \sim R_x + R_e/p\tau_1 \sim R_e/p\tau_1$$
$$[\text{Capacitive for } \omega \ll (R_x C_d)^{-1}] \qquad [21]$$

$$Z_T \sim R_x \quad [\text{Resistive for } \omega \gg (R_x C_d)^{-1}] \qquad [22]$$

3. Finally, at high frequencies, such that $\omega \gg \omega_a'$, this leads to

$$Z_T \sim R_x + R_e/\sqrt{p\tau_1} \sim R_e/\sqrt{p\tau_1} \quad \text{if } \omega \ll (R_e/R_x)^2/\tau_1 \qquad [23]$$

$$Z_T \sim R_x \quad \text{if } \omega \gg (R_e/R_x)^2/\tau_1 \qquad [24]$$

The phase angles predicted by the limits described through Eq. 19-24 are depicted in the following schematic. These results show that the phase angles are predicted to change, from 0, to 45, 90, 0, and then to 90° again, as the frequency, ω, is lowered.

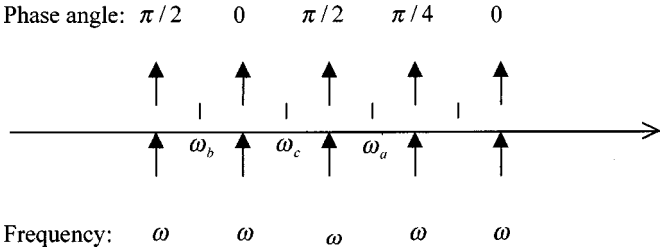

It should be noted here that the phase angle of 45°, while predicted by Eq. 23, can also arise when $R_t C_\varphi \gg 1$, *i.e.*, when

$$U(p) = \sqrt{pR_e C_d + \frac{R_e}{R_t}} \qquad [25]$$

When R_e/R_t is small compared to $R_e C_d$ and when ω is high, $Z(p)$ is proportional to $1/\sqrt{j\omega}$, which is π/4. However, it should be noted that while this feature is theoretically possible, it may not be experimentally accessible.

Their phase angle/frequency schematic presented shows that as the frequency decreases, a maximum appears in the phase angle plots in the intermediate frequency region as a result of the interpositioning of the various time constants with respect to frequency. In other words, the appearance of maxima in the phase angle plots is a consequence of the charging of the porous oxide film double layer first and then the pseudocapacitance, at different times in the porous matrix. At high frequencies, the double layer is charged, the time

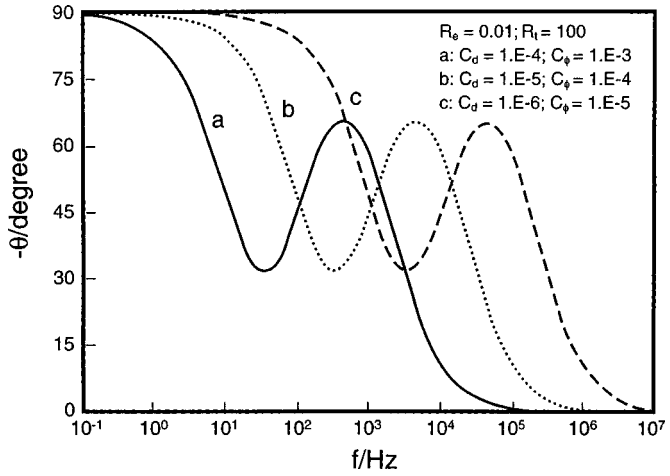

Figure 9. Theoretical phase angle plots using Eq. 12 and 13 for $R_e = 10^{-2}$ and $R_t = 100$, along with the relevant ω values.

	C_d	C_φ	ω_a	ω_b	ω_c
(a)	10^{-4}	10^{-3}	10^5	10	10^2
(b)	10^{-5}	10^{-4}	10^6	10^2	10^3
(c)	10^{-6}	10^{-5}	10^7	10^3	10^4

constant associated with it being R_tC_d. As the frequency is lowered, the pseudocapacitor is charged, with the time constant for this process being R_tC_ϕ, ultimately resulting in the phase angle of 90° as $\omega \rightarrow 0$, These variations are depicted in Fig. 9 and 10, as a function of a variety of combinations of magnitudes of the circuit elements, for the inequalities in the τ values stated.

It should be noted that the inequalities indicated in the cases presented must be satisfied (even if the $\gg$ or $\ll$ conditions are not strictly satisfied) for the appearance of maxima or minima in the phase angle plots. It should also be emphasized here again that the development of peaks in the phase angle plots is a consequence of

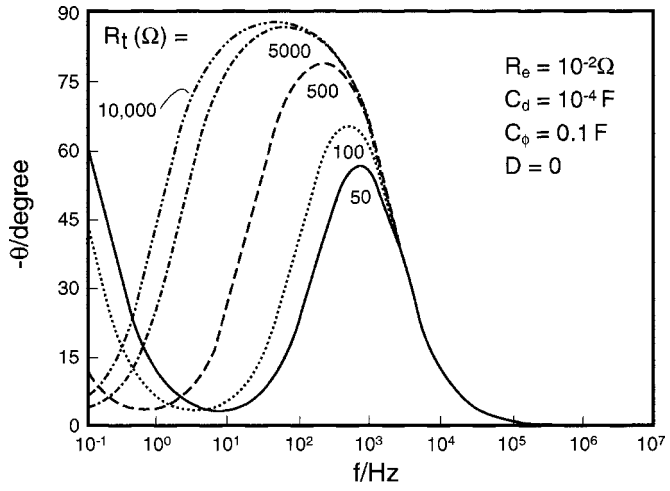

Figure 10. Theoretical phase angle plots using Eq. 12 and 13 for $R_e = 10^{-2}$, $C_d = 10^{-4}$, and $C_\phi = 0.1$, along with the pertinent ω values.

	R_t	ω_a	ω_b	ω_c
(a)	50	10^3	0.2	200
(b)	100	10^3	0.1	100
(c)	500	10^3	0.02	20
(d)	5,000	10^3	0.01	10
(e)	10,000	10^3	0.001	1

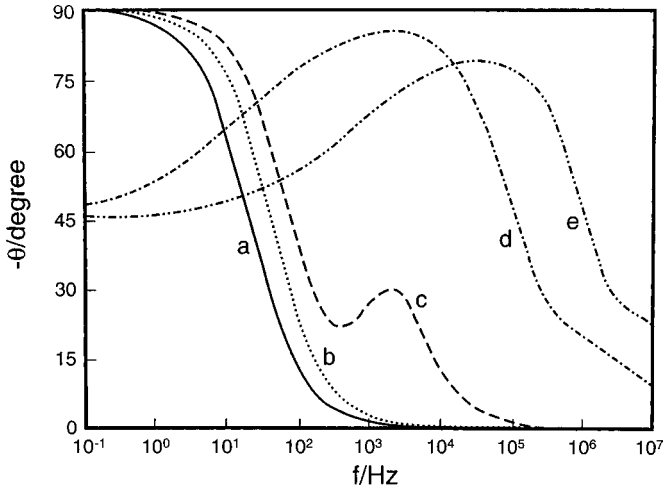

Figure 11. Theoretical phase angle plots using Eq. 12 and 13 for a, b, and c, and Eq. 12 and 29 for d and e.

	R_e	C_d	C_φ	R_t	D
(a)	10^{-2}	10^{-4}	10^{-2}	3×10^{-2}	0
(b)	10^{-2}	10^{-4}	5×10^{-3}	10^{-1}	0
(c)	10^{-2}	10^{-4}	10^{-3}	10	0
(d)[a]	15	10^{-6}	10^{-7}	2×10^2	6.5×10^{-5}
(e)[a]	20	10^{-7}	10^{-8}	10^3	6.5×10^{-5}

[a] C_φ for these cases is equal to the value noted divided by $(a_1 + 1)$.

the interplay of the time constants, dictated by the impedance function given in Eq. 12 and 13.

Dependence of impedance response on Ru content of film.—The comparison of the calculated and experimental impedance plots must also be carried out in terms of the Ru content in the film. This brings in the question of the parametric dependence on θ_{RuO_2} (where θ_{RuO_2} is the surface coverage by redox-active Ru surface sites). The terms C_d, C_ϕ, R_t, and R_e in Eq. 13 can all be assumed to be related to the number of active RuO_2 sites in the Ru/Ti oxide coating, although this must be accepted with some caution, as the fundamental relationships are more complex and nonlinear. Nevertheless, it is usual to assume that the following parameters, C_ϕ, $1/R_t$, and C_d are all proportional to θ_{RuO_2}. This is based on the assumptions that the only source of pseudocapacitance is the Ru^{3+}/Ru^{4+} surface redox process and that i_o varies linearly with θ_{RuO_2}. In addition, R_e also varies with θ_{RuO_2}, since $\ln \sigma_m = (\theta_{RuO_2}/\theta_{TiO_2} \ln \sigma_{RuO_2})$, where $\sigma_m = 1/R_m$ and σ_{RuO_2} and σ_{TiO_x} refer to the conductivity of RuO_2 and TiO_x, respectively. The suggested linear relationship between $C_d \propto \theta_{RuO_2}$ implies that the double-layer capacity of RuO_2 is very different (higher) than that of TiO_x, so that the number of Ru surface sites dominate the measured interfacial capacitance. It should also be noted that R_e, the overall matrix resistance, increases, while the C_d and C_ϕ terms decrease, with a decrease in the number of active Ru sites in the film.

Figure 11 (curves a-c) depicts the calculated phase angle data (Eq. 12) using circuit element values which might be typical of freshly formed 40, 30, and 20 atom % Ru coatings. R_e is very small, as these oxides are expected to be very conductive, so that the matrix resistance is very low. The C_d and C_φ values are both quite high, as the Ru content is high. The R_t value of 0.03 Ω and C_ϕ of 0.01 F (curve a, 40% Ru), chosen for these calculations, is consistent with the values reported[27] for high Ru atomic percent electrodes. When the Ru content in the coating decreases, the adsorption pseudocapacitance decreases, and the charge-transfer resistance as-

sociated with the faradaic process of Eq. 1 increases. This is consistent with the rationale of the lowered number of active Ru sites and hence lower faradaic currents under these conditions.

Inclusion of diffusion-controlled process in simulation.—It can be seen that Eq. 12 cannot completely describe the behavior of the low Ru atomic percent electrodes, which show a phase angle of 45-60° at very low frequencies (Fig. 6) and a broad hump in the mid- to high-frequency region. It should be noted that Eq. 12 can account only for the phase angle variations in the frequency region of 10^6-10^2 Hz. Therefore, some modifications to the model were explored and a search for additional phenomenological and/or reaction steps, which may have been missed in the simple assumed mechanism, was undertaken. This led to the consideration of two other possible reactions.

The first is that of a parasitic or poisoning step, involving the poisoning of the surface by species Z*, specifically of one of the two surface redox states (Ru^{+3} = R; Ru^{+4} = O) of Ru oxide. As a result, $O_{ad} + ne + Z^* \leftrightharpoons R^*$, for example, would occur in parallel with $O_{ad} + ne \rightleftharpoons R_{ad}$. The analysis for this situation leads to an impedance expression which is similar to Eq. 12, but with $U(p)$ given by

$$U(p) = \sqrt{\frac{1}{\sigma''}\left(pA + \frac{pB^* + D^*}{1 + pC^* + k/p}\right)} \qquad [26]$$

where

$$A = R_e C_d$$

$$B^* = \frac{n^2F^2}{RT}(\beta i_o^* + i_o)z$$

$$C^* = nFZ$$

$$D^* = \frac{nF}{RT}\frac{\beta i_o i_o^*}{\Gamma_R^o}Z$$

$$k = \frac{i_o i_o^*}{nF\Gamma_O^o\Gamma_R^o}Z$$

$$Z = \left[i_o\left(\frac{1}{\Gamma_O^o} + \frac{1}{\Gamma_R^o}\right) + \frac{i_o^*}{\Gamma_O^o}\right]^{-1}$$

and where β is the transfer coefficient for the forward rate of the parasitic reaction, and i_o^* is the exchange current density of the parasitic reaction.

A second possible explanation for the observed phase angles of 40-60° at low frequencies (see Fig. 5 and 6) involves concentration polarization effects. These could be associated with transport control of the H^+ reacting with the Ru^{4+} sites, or to diffusion control of oxygen to the electrode surface, prior to its reduction on low atom percent Ru electrodes. This presents additional difficulties in the analysis, and the coupling of concentration and potential variations leads to complex expressions, so that a detailed analysis is not presented here. An approximate[e] analysis,[45] which relates the concentration changes to the potential, leads to

$$\frac{\Delta C_X}{C_X^o} \approx \frac{nF}{RT}\Delta\phi\left(\frac{a_o}{\sqrt{p}} + a_1 + a_2\sqrt{p} + \ldots\right) \qquad [27]$$

When Eq. 27 is substituted into the linearized rate Eq. 28 for Reaction 1, the impedance expression can be shown to be the same as Eq. 12, with the $U(p)$ term expressed by Eq. 29

[e] It is interesting to note that the results obtained here can be deduced from those given in Ref. 43 and 44 by allowing the diffusion coefficient $\rightarrow 0$. Thus, the generalization of Eq. 12 to account for the presence of a diffusion-controlled process at low frequencies is possible.

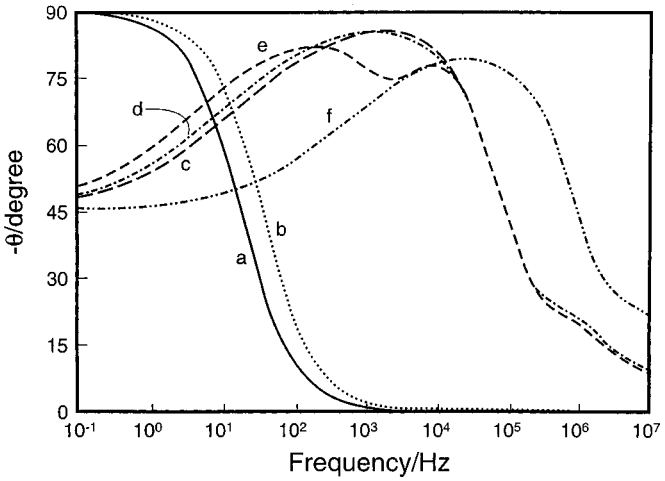

Figure 12. Theoretical phase angle plots simulating the experimental Bode plots during deactivation using Eq. 12 and 29.

	R_e	C_d	C_φ	R_t	D
(a)	10^{-2}	10^{-4}	10^{-2}	3×10^{-2}	0
(b)	10^{-2}	10^{-4}	5×10^{-3}	10^{-1}	0
(c)[a]	15	10^{-6}	10^{-7}	2×10^{2}	6.5×10^{-5}
(d)[a]	18	10^{-6}	10^{-7}	5×10^{2}	6.5×10^{-5}
(e)[a]	20	10^{-6}	5×10^{-7}	10^{3}	67.5×10^{-5}
(f)[a]	20	10^{-7}	10^{-8}	10^{3}	6.5×10^{-5}

[a] C_φ for these cases is equal to the value noted divided by $(a_1 + 1)$.

$$-nF\frac{d\Delta\Gamma_O}{dt} = i_o\left[\frac{\Delta C_X}{C_X^o} + \left(\frac{1}{\Gamma_O^o} + \frac{1}{\Gamma_R^o}\right)\Delta\Gamma_O + \frac{nF}{RT}\Delta E\right] \qquad [28]$$

$$U(p) = \sqrt{\frac{1}{\sigma''}\left(pA + \frac{pB' + D\sqrt{p}}{1 + pC}\right)} \qquad [29]$$

where

$$A = R_e C_d$$

$$B' = R_e C_\phi (1 + a_1)$$

$$C = R_t C_\phi$$

$$D = R_e C_\phi a_o$$

The expressions appropriate to poisoning of the surface and the inclusion of a diffusion-controlled process have been tested for fit with the experimental phase angle plots. It is found that allowing for concentration polarization effects duplicates the experimental Bode plots well, as shown later. The exact nature of the diffusion process and the identify of the species contributing to this Warburg-like behavior will be discussed elsewhere.

The simulation results, shown in Fig. 11 (curves d and e), demonstrate that the incorporation of a diffusional process in the case of freshly formed, low atom percent Ru coatings does indeed describe the experimental phase angle behavior (cf. Fig. 6) well. The results in Fig. 11, thus, show that as the atom percent Ru decreases, for freshly formed films, C_ϕ decreases and R_t increases, and a maximum develops in the phase angle plots. At low atom percent Ru levels, diffusion of either H^+ in the Ru/Ti oxide solid state, or diffusion of trace species, such as oxygen, to the electrode surface, can now be detected in the impedance data, and the phase angle then approaches 45° at low frequencies.

An analogous approach was made to attempt a good simulation of the impedance data for deactivated electrodes using the data for a

30 atom percent Ru film (Fig. 5). Figure 12 shows the phase angle Bode plots, based on a range of circuit element values and including the low-frequency diffusional term, *D*. These results show that, with time of electrode deactivation, the 30 atom percent Ru electrode increasingly behaves like a low atom percent Ru electrode (Fig. 6). The appearance of a maximum in the phase angle plots at high frequencies as deactivation begins to occur is the result of *a* decreasing C_ϕ and an increasing R_t. This demonstrates clearly that Ru depletion has occurred, as these changes in the circuit elements could not be the result of a resistance buildup at the Ti/coating interface.

Overall, the Tafel, the cyclic voltammetric rresults, and the ac impedance data all suggest that when a RuO_2/TiO_2 anode exhibits high overpotential, this is a direct consequence of the surface depletion of Ru. This is also consistent with the estimated R_e values of $\sim$20 Ω for the failed electrodes, in contrast to the known high specific resistivity of TiO_2 of 10^{13} Ω cm, which would suggest the absence of any buildup of a TiO_2 layer at the Ti and the Ru/Ti coating when anode deactivation occurs. It should particularly be noted, as a piece of additional evidence supporting the absence of the buildup of a TiO_2 layer, that a failed electrode gives the same frequency response as a fresh 5% Ru electrode at low frequencies.

The University of Calgary assisted in meeting the publication costs of this article.

List of Symbols

C_d	double-layer capacitance, F/cm^2
C_ϕ	pseudocapacitance, F/cm^2
F	Faraday constant
j	$\sqrt{-1}$
l	pore length
n	number of electrons involved in the overall reaction
p	Laplace transfer variable $= j\varpi$
R_e	matrix resistance, Ω
R_t	charge-transfer resistance, Ω
s	surface area of porous electrode per unit length
x	distance coordinate in the direction normal to the electrode surface

Greek

ϕ	electrode potential
ϖ	ac frequency
θ	surface coverage of the species in the subscript
Γ	surface excess of the species in the subscript

Subscripts

O	oxidant
R	reductant

Superscripts

o	value at $\phi = 0$

References

1. S. Trasatti, *The Electrochemistry of Novel Materials*, J. Lipkowski and P. N. Ross, Editors, p. 207, VCH Publishers, New York (1994).
2. B. E. Conway and B. V. Tilak, in *Fundamentals of Electrochemical Process Design: A Tutorial*, J. B. Talbot, B. E. Conway, J. M. Fenton, and B. V. Tilak, Editors, PV 95-11, p. 319, The Electrochemical Society Proceedings Series, Pennington, NJ (1995).
3. R. C. Carlson, Paper presented at the 14th Annual Chlorine-Chlorate Seminar, Eltech Systems Corporation, Chardon, OH (1998).
4. Yu. B. Makarychev, E. K. Spasskaya, S. D. Khodkevich, and L. M. Yakimenko, *Elektrokhimiya*, **12**, 994 (1976).
5. T. Loucka, *J. Appl. Electrochem.*, **7**, 211 (1977).
6. A. A. Uzbekov, V. G. Lambrev, I. F. Yazikov, N. N. Rodin, L. M. Zabrodskaya, V. S. Klement'eva, and Yu. M. Vlodov, *Elektrokhimiya*, **14**, 1150 (1978).
7. V. V. Gorodetskii, M. M. Pecherskii, V. B. Yanke, D. M. Shub, and V. V. Losev, *Elektrokhimiya*, **15**, 559 (1979).
8. F. Hine, M. Yasuda, T. Noda, T. Yoshida, and J. Okuda, *J. Electrochem. Soc.*, **126**, 1439 (1979).
9. C. Iwakura, M. Inai, M. Manabe, and T. Tamura, *Denki Kagaku*, **48**, 91 (1980).
10. T. Loucka, *J. Appl. Electrochem.*, **11**, 143 (1981).
11. V. V. Gorodetskii, M. M. Pecherskii, V. B. Yanke, N. Ya. Bun'e, V. B. Busse-Machukas, V. L. Kubasov, and V. V. Losev, *Elektrokhimiya*, **17**, 513 (1981).
12. A. A. Uzbekov and V. S. Klement'eva, *Elektrokhimiya*, **21**, 758 (1983).
13. M. D. Spasojevic, N. V. Krstajjic, and M. M. Jaksic, *J. Res. Inst. Catalysis*, **31**, 77 (1983).
14. C. Iwakura and K. Sakamoto, *J. Electrochem. Soc.*, **132**, 2420 (1985).
15. V. S. Klement'eva and A. A. Uzbekov, *Elektrokhimiya*, **21**, 796 (1985).
16. M. M. Pecherskii, V. V. Gorodotskii, N. Ya. Bun'e, and V. V. Losev, *Elektrokhimiya*, **22**, 656 (1986).
17. V. I. Eberil, N. V. Zhinkin, V. P. Archakov, R. I. Izosenkov, V. B. Busse-Machukas, and A. F. Mazanko, *Elektrokhimiya*, **33**, 459 (1986).
18. N. V. Zhinkin, E. A. Novikov, N. S. Fedotova, V. I. Eberil, and V. B. Busse-Machukas, *Elektrokhimiya*, **25**, 1094 (1989).
19. S. V. Evdokimov and K. A. Misheninaa, *Elektrokhimiya*, **25**, 1605 (1989).
20. S. Manli and C. Yanxi, *Modern Chlor-Alkali Technology*, Vol. 4, p. 149, N. M. Prout and J. S. Moorehouse, Editors, Elsevier Applied Science, New York (1990).
21. E. A. Novikov, N. V. Zhinkin, V. I. Eberil, and B. Busse-Machukas, *Elektrokhimiya*, **26**, 245 (1990); E. V. Novikov and V. Busse-Machukas, *Elektrokhimiya*, **27**, 116 (1991).
22. A. S. Pilla, E. O. Cobo, M. M. E. Duarte, and D. R. Salinas, *J. Appl. Electrochem.*, **27**, 1283 (1997).
23. C. E. Vallet, B. V. Tilak, R. A. Zuhr, and C.-P. Chen, *J. Electrochem. Soc.*, **144**, 1289 (1997).
24. K. L. Hardee and R. A. Kus, in *Modern Chlor-Alkali Technology*, Vol. 7, p. 43, S. Sealey, Editor, Published for SCI by the Royal Society of Chemistry, Cambridge, U.K. (1998).
25. V. V. Gorodetskii, P. N. Zorin, M. M. Pechereskii, V. B. Busse-Machukas, V. L. Kubasov, and Yu. Ya. Tomashpolskii, *Elektrokhimiya*, **17**, 79 (1981).
26. P. H. Duvigneaud and A. Coussment, *J. Solid State Chem.*, **52**, 22 (1984).
27. E. D. Spasskaya, Yu. B. Makarychev, A. A. Yakovleva, and L. M. Yakimenko, *Elektrokhimiya*, **13**, 227 (1977).
28. W. A. Gerrard and B. C. H. Steele, *J. Appl. Electrochem.*, **8**, 417 (1978).
29. C. E. Vallet, D. A. Heatherly, and C. W. White, *J. Electrochem. Soc.*, **137**, 5479 (1990).
30. C. E. Vallet, *J. Electrochem. Soc.*, **138**, 1234 (1991).
31. M. Pourbaix, *Atlas of Electrochemical Equilibria in Aqueous Solutions*, NACE, Houston, TX (1974).
32. T. V. Bommaraju, C.-P. Chen, and V. I. Birss, *Modern Chlor-Alkali Technology*, Vol. 8, Royal Society of Chemistry, London (2001).
33. C. E. Vallet, *Appl. Phys. A: Mater. Sci. Process.*, **65**, 387 (1997).
34. C. A. Gervasi and J. R. Vilche, *Electrochim. Acta*, **37**, 1389 (1992).
35. S. G. Seal, J. R. Vilche, and A. J. Arvia, *J. Electroanal. Chem.*, **341**, 181 (1992).
36. E. B. Castro, S. G. Seal, R. H. Milocco, and J. R. Vilche, *Electrochim. Acta*, **36**, 117 (1991).
37. B. V. Tilak, C.-P. Chen, V. I. Birss, and J. Wang, *Can. J. Chem.*, **75**, 1773 (1997).
38. S. Trasatti and P. Kurzweil, *Platinum Met. Rev.*, **38**, 46 (1994).
39. B. E. Conway, *J. Electrochem. Soc.*, **138**, 1539 (1991).
40. B. V. Tilak, C.-P. Chen and S. K. Rangarajan, *J. Electroanal. Chem.*, **324**, 405 (1992) and **356**, 319 (1993).
41. B. E. Conway and B. V. Tilak, *Adv. Catal.*, **38**, 1 (1992).
42. B. Pillay and J. Newman, *J. Electrochem. Soc.*, **143**, 1806 (1996).
43. S. K. Rangarajan, *J. Electroanal. Chem.*, **22**, 89 (1969) and **41**, 459 (1973).
44. R. De Levie, in *Advances in Electrochemistry and Electrochemical Engineering*, P. Delahay, Editor, Vol. 6, p. 329, Interscience, New York (1967).
45. S. K. Rangarajan, Unpublished results (1999).